European Cells and Materials Vol.52 2025 (pages 44–57) DOI: 10.22203/eCM.v052a04 ISSN 1473-2262

Original Article

GENERATION OF THREE-DIMENSIONAL (3D) BREAST CANCER BONE METASTASIS MODEL FOR DRUG TESTING

H. Nasser[1,2,3,*], A. Aszodi[1], S. Otto[3] and R. Fliefel[1,3,4,*]

[1]Department of Orthopaedics and Trauma Surgery, Musculoskeletal University Center Munich (MUM), Ludwig-Maximilians-University (LMU), 81252 Planegg, Germany

[2]Department of Oral and Maxillofacial Surgery, Faculty of Dentistry, Cairo University, 11553 Cairo, Egypt

[3]Department of Oral and Maxillofacial Surgery and Facial Plastic Surgery, University Hospital, Ludwig-Maximilians-University (LMU), 80337 Munich, Germany

[4]Department of Oral and Maxillofacial Surgery, Faculty of Dentistry, Alexandria University, 21521 Alexandria, Egypt

Abstract

Background: In cancer research, the multicellular tumour spheroids (MCTSs) model has attracted great attention as a transitional stage between *in vitro* two-dimensional (2D) cultures and *in vivo* studies, contributing to a better understanding of tumour biology. The objective of this study was to construct three-dimensional (3D) homotypic bone and cancer spheroids together with heterotypic spheroids resembling breast cancer metastasis to the bone. **Methods**: To construct spheroid models, cells were seeded in ultra-low attachment (ULA) plates with varying concentrations of Matrigel followed by forced aggregation via centrifugation. The models were validated by growth kinetics, cell viability and quantitative real-time polymerase chain reaction (RT-qPCR). **Results:** The addition of Matrigel allowed the formation and growth of the spheroids. Matrigel enhanced the circularity of the spheroids for homotypic cancer spheroids but significantly reduced their viability. Matrigel had the opposite effect on homotypic bone spheroids, significantly improving viability and negatively affecting circularity. The formation of heterotypic spheroids with 1 % Matrigel represented the optimum condition with high viability and circularity index. The model was subsequently validated to accurately represent bone metastasis via the upregulation of the pro-metastatic genes. **Conclusions**: Incorporating Matrigel as an extracellular matrix (ECM) protein mixture into spheroid models is crucial as it enhances cellular interactions and is the key to simulating *in vivo* conditions. Consequently, we constructed a 3D heterotypic tumour spheroid model using 1 % Matrigel as a robust and versatile model to study different aspects of breast cancer metastasis to the bone and for further drug testing.

Keywords: Bone, metastasis, breast cancer, extracellular matrix, spheroids, three-dimensional, Matrigel, osteoblasts.

***Address for correspondence**: H. Nasser, Department of Orthopaedics and Trauma Surgery, Musculoskeletal University Center Munich (MUM), Ludwig-Maximilians-University (LMU), 81252 Planegg, Germany; Department of Oral and Maxillofacial Surgery, Faculty of Dentistry, Cairo University, 11553 Cairo, Egypt; Department of Oral and Maxillofacial Surgery and Facial Plastic Surgery, University Hospital, Ludwig-Maximilians-University (LMU), 80337 Munich, Germany. E-mail: Nasser.Mansour@med.uni-muenchen.de; R. Fliefel, Department of Orthopaedics and Trauma Surgery, Musculoskeletal University Center Munich (MUM), Ludwig-Maximilians-University (LMU), 81252 Planegg, Germany; Department of Oral and Maxillofacial Surgery and Facial Plastic Surgery, University Hospital, Ludwig-Maximilians-University (LMU), 80337 Munich, Germany; Department of Oral and Maxillofacial Surgery, Faculty of Dentistry, Alexandria University, 21521 Alexandria, Egypt. E-mail: Riham.Fliefel@med.uni-muenchen.de.

Introduction

Breast cancer (BC) is the most commonly diagnosed malignancy, leading to the second highest number of cancer-related deaths in women after lung cancer [1,2]. Metastasis is a fatal complication in which the breast cancer cells spread beyond the primary tumour to the nearby lymph nodes and other organs [3]. Among the various sites of breast cancer metastasis, bone is the most common site where cancer cells infiltrate the microenvironment and disrupt the normal structure of the bone. Skeletal-related events (SREs) such as bone pain, fractures and spinal compression are complications associated with BC bone metastasis, which seriously affect patients' quality of life and disease prognosis [4].

The survival rates of patients with primary breast cancer have greatly improved over the past decades, in contrast, survival rates have decreased in patients with metastatic breast cancer, with 5-year survival rate as low as 38 % de-

pending on the extent of metastasis and the presence of SRE [5]. Although metastasis to the maxillofacial bones is less common than metastasis to long bones, it is indicative of the late stage of the disease and the presence of metastases at other sites [6].

Once breast cancer metastasizes to distant regions, it becomes resistant to treatment due to genetic alterations in the metastasizing cells together with interactions with the metastatic site, increasing susceptibility to therapy. Accordingly, the management of metastatic breast cancer is remarkably more complicated than that of primary BC [7].

Despite the clinical importance of metastasis, research has focused principally on primary tumours, and much remains missing concerning the metastatic process. This has prompted researchers to develop preclinical models reflecting the complexity of the molecular microenvironment with a deeper understanding of the metastatic cascade, which may facilitate the development of new treatment strategies that could improve cancer survival rates [8,9].

To study breast cancer metastasis to bone, several *in vitro* and *in vivo* models have been used [10]. However, *in vivo* animal models are highly restrictive because they are expensive, raise ethical issues, and often, animals die before bone metastasis occurs [11,12]. For these reasons, there is great interest in replacing animal models with *in vitro* or *ex vivo* models, as society and authorities are increasing the pressure to find substitutes for experimental animals, as evidenced by the Humane Research and Testing Act (HR 1744) and the US Food and Drug Administration (FDA) Modernization Act of 2021 [13].

Currently, research has introduced a variety of *in vitro* cancer models, including abundant two-dimensional (2D) and three-dimensional (3D) models, ranging from simple tissue culture Petri dishes, flasks or transwells to more elaborate hydrogels, scaffolds or spheroids, among others that mimic the *in vivo* environment [14].

Compared with conventional 2D cultures, tumour cells maintained in 3D models show characteristics that better represent their *in vivo* behavior [15]. Spheroid models have been applied to represent the complexity and cellular characteristics of tumours for drug testing, filling the gap between *in vivo* studies and 2D models [16,17].

Multicellular tumour spheroids (MCTSs) are 3D models that consist of cell aggregates that are either homotypic, comprising only one cell type, or more complex heterotypic structures from the co-culture of two or more cell types formed either by self-assembly or forced aggregation [18].

Recently, the MCTS model has been recognized as a transitional phase between *in vitro* 2D cultures and *in vivo* studies in cancer research that are devoted to obtaining better insight into tumour biology. Compared with 2D monolayer cell cultures, MCTSs closely imitate several features of *in vivo* tumours, such as growth kinetics, the oxygen gradient, tumour configuration, pH, metabolic rates and resistance to radiotherapy or chemotherapy [19].

Unfortunately, the use of different construction techniques might result in the formation of cell aggregates but not true tumour spheroids. Thus, it is essential to introduce additives to enhance the proper formation of MCTSs [20]. The additives facilitate MCTS formation, increasing their structural stability and increasing their biological relevance [21]. In particular, Matrigel has been introduced as a natural scaffold material for 3D cultures of many cell types providing high efficiency in the generation of tight cell-cell interactions and cell-extracellular matrix (ECM) interactions that are implicated in the regulation of signaling pathways and the induction of cellular responses [22]. Multicellular spheroids cultivated with Matrigel demonstrate complex cellular behavior that is otherwise difficult to achieve through other culture approaches [23].

Therefore, the overall goal of this study was to (a) construct 3D homotypic bone and cancer spheroids and a heterotypic spheroid model system resembling breast cancer metastasis to the bone; (b) validate the model in terms of generation time, growth kinetics, morphological characteristics and cell viability, and (c) demonstrate the effect of cancer and bone cell co-culture at the RNA level.

Materials and Methods

Culture of Human Osteoblasts (hOBs) and Breast Adenocarcinoma Cell Line (MDA-MB-231)

Primary human osteoblasts (hOBs) were purchased from PromoCell (C-12720, Heidelberg, Germany). A human breast adenocarcinoma cell line (MDA-MB-231; HTB-26, ATCC, Manassas, VA, USA) was kindly donated by Professor Hanna Taipaleenmäki. The cells were cultured in complete culture media consisting of Dulbecco's modified Eagle medium high glucose (DMEM-HG; P04-04515, PAN Biotech, Aidenbach, Germany) supplemented with 15 % fetal bovine serum (AC-SM-0161Hi, Anprotec, Bruckberg, Germany) and 1 % penicillin/streptomycin (P0781, Sigma Aldrich, Taufkirchen, Germany) and grown at 37 °C in a 5 % CO_2 atmosphere.

The culture media was replaced twice per week, and the cells were trypsinized at 80–90 % confluency using 1X Trypsin (0.25 % trypsin/0.53 mM ethylenediaminetetraacetic acid (EDTA) solution 59418C, Sigma Aldrich, Taufkirchen, Germany). The osteoblasts between passages 5 and 10 were used from two different donors, whereas the MDA-MB-231 cells were passaged until sufficient cells were acquired for the experiments for no more than 10 passages to avoid the phenotypic drift. Untransfected MDA-MB-231 cells were used throughout the experiments unless otherwise reported.

Misidentification of the cell line was checked at the Register of Misidentified Cell Lines and the chosen cell line was not on the list [24]. The extracted DNA from the cell line was sent to Eurofins Genomics (Ebersberg, Germany) for authentication via DNA and short tandem repeat-profiles. Authentication confirmed the correct identity of

the cell line and each used cell type tested negative for mycoplasma contamination.

Generation of Multicellular Homotypic/Heterotypic Spheroids

Homotypic MDA-MB-231 or hOBs spheroids were generated by seeding the cells at a density of 1×10^4 cells/200 μL of culture media. Heterotypic multicellular tumour spheroids were generated by the co-culture of MDA-MB-231 cells and hOBs at a ratio of 1:1 (5×10^3 cells for each cell type). Three-dimensional cultures were generated in the presence of either 1 % or 3.5 % (v/v) Matrigel basement membrane matrix (356237, Corning, Corning, NY, USA) in complete culture medium. The cells cultured in the absence of Matrigel served as controls.

Briefly, Matrigel was first thawed overnight at 4 °C in the refrigerator along with pipette tips to prevent premature polymerization during handling. After thawing, the Matrigel was added directly to the cell suspension to achieve the desired final concentrations (1 % and 3.5 %).

Ultra-low attachment (ULA) 96-well round-bottom plates (BIOFLOAT, 83.3925.400, Sarstedt AG., Nümbrecht, Germany) were used to promote the aggregation of the cells into 3D spheroids. The cells were condensed at the rounded bottom of the 96-well plates by centrifugation at 410 × g for 10 min at 25 °C (5430 R, Eppendorf, Hamburg, Germany). The plates were then incubated at 37 °C and 5 % CO_2 in humidified incubators to maximize cell-cell adhesion. The culture media was changed the next day by replacing half of the culture media with fresh media and incubating for 48 hours in a humidified atmosphere of 5 % CO_2 at 37 °C to allow cells to grow and form the spheroids.

Monitoring Morphology and Spheroid Growth Kinetics

Spheroid formation was studied in terms of the morphological changes expressed as spheroid diameter and circularity (Cir) as a function of time. Spheroid growth was monitored from Day 0 (i.e., 48 hours after the beginning of the spheroid culture) to Day 14. A 50 % medium supplemented with Matrigel was added on Days 3, 7 and 10. To examine the growth of spheroids over time, spheroids from each condition were imaged at different time points via the 5X objective of a light microscope (Zeiss Axio Vert.A1, Carl Zeiss AG, Oberkochen, Germany) coupled with a Zeiss Axiocam Icm1 Monochrome Camera (Carl Zeiss AG, Oberkochen, Germany). All the images were analysed via the open-source software ImageJ (1.54j 12 June 2024, National Institutes of Health, Bethesda, MD, USA, https://imagej.nih.gov/ij/).

Morphological analysis of the spheroids was performed on calibrated images by applying images of a known scale for calibration. This was achieved by selecting the "set scale" option in the analyse menu. Afterwards, the length of the scale bar was measured in μm and the scale was applied globally to ensure that it was used for all subsequent images. The "set measurements" option was used to select the parameters of interest where Feret's diameter was used to estimate the mean diameter of the spheroids and the circularity index was selected. Additionally, the polygonal tool was used to outline the spheroids such that the projected diameter and circularity were obtained. The parameter "Circularity" (Cir) was used as a shape descriptor to calculate the sphericity index (SI), which could mathematically indicate the degree of similarity of the spheroids to a perfect circle [25] and was calculated according to the following equation:

$$\text{Circularity} = 4\pi \times \frac{\text{Area}}{\text{Perimeter}^2} \quad (1)$$

A value of 1.0 indicates a perfect circle, whereas a value approaching 0.0 indicates an increasingly elongated shape.

Live/Dead Fluorescence Staining Assay for 3D Cultures

The viability of the homotypic and heterotypic spheroids was assessed via a live/dead viability/cytotoxicity kit (L3224, Thermo Fisher Scientific, Darmstadt, Germany) according to the manufacturer's instructions at Days 0 and 7 via Calcein acetoxymethylester (Calcein-AM) (green fluorescence for live cells) and ethitium homodimer-1 (red fluorescence for-dead cells).

Briefly, the media was carefully aspirated from the microwells, and the spheroids were washed with 1X phosphate buffer saline (PBS). Next, 80 μL of the live/dead staining solution was added to each well, followed by incubation at 37 °C with 5 % CO_2 for 60 min in the dark. Afterwards, the spheroids were rewashed with PBS to remove the unbound dyes and kept in PBS for imaging by a fluorescence microscope (Zeiss Axio Observer Z1, Carl Zeiss AG, Oberkochen, Germany) with a dry 10X magnification objective lens. Images were captured by CY3 and GFP filters and merged.

Quantification of Live/Dead Staining

The percentage of viability within the spheroids was determined as the ratio of the fluorescence intensity of the viable cells to the total fluorescence intensity of the spheroids. The fluorescence intensity was measured via the total corrected cellular fluorescence (TCCF) method [26]. Following the live/dead staining of the spheroids, the fluorescence images were imported into ImageJ software, where the green and red channels were separated. The integrated density (ID) of the areas of interest was calculated on each channel separately. The TCCF of viable cells was measured as follows:

$$\text{TCCF (viable)} = \text{ID (green)} - (\text{Area} \times \text{mean ID background}) \quad (2)$$

TCCF for the dead cells was calculated following the same equation using the integrated density in the red channel. The total TCCF represents the sum of both channels. The percentage of viable cells was calculated as follows:

$$\text{Viability } \% = \left(\frac{\text{TCCF viable}}{\text{TCCF total}}\right) \times 100 \quad (3)$$

Transfection of MDA-MB-231 Cells

For confocal imaging, MDA-MB-231 cells at 70–80 % confluence were nucleofected (VCA-1003, Amaxa™ Cell Line Nucleofector™ Kit V, Lonza, Basel, Switzerland) by the Sleeping Beauty transposon system as previously described [27] using the pSBbi-RFP transposon plasmid and the pCMV(CAT)T7-SB100 ecoding the transposase. At 48 hours post-transfection, the cells were selected with 1.5 μg/μL puromycin (P7255, Sigma Aldrich, St. Louis, MO, USA) for one week to eliminate non-stable nucleofected cells. For further purification, the cells were sorted by fluorescence-activated cell sorting (FACS; BD FACSAria™ III, BD Biosciences, Heidelberg, Germany) according to their red fluorescent protein (RFP) expression. Finally, the cells were incubated for three days at 37 °C and 5 % CO_2. Untransfected cells were used as the negative control. The cell populations were sorted twice by the FACS to obtain high percentages of stably nucleofected cells with medium-high RFP expression.

Vital Cell Labelling of hOBs

Vital cell labelling of hOBs was carried out using the Lipophilic Vybrant 3,3′-Dioctadecyloxacarbocyanine perchlorate (DIO) cell labelling solution (Molecular Probes, Leiden, Netherlands) on the same day of spheroid culture. DIO-labelled osteoblasts were utilized for confocal imaging of the homotypic and heterotypic spheroids. Briefly, the cells were trypsinized, counted, and suspended at a density of 1×10^6cells/mL in serum-free culture medium, and 5 μL of 1 mM DIO dye solution was added to each 1 mL of cell suspension and mixed well by gentle pipetting. The cells were incubated in the dark for 20 min at 37 °C in a humidified incubator under 5 % CO_2. The labelled suspension tubes were centrifuged at 1500 rpm for 5 min at 37 °C. The supernatant was removed, and the cell pellet was gently re-suspended in a warm culture medium (37 °C). The cells were washed in the culture media two times. Stably nucleofected and FACS-sorted RFP-MDA-MB-231 cells, together with the labelled hOBs were used for the fabrication of either homotypic or heterotypic spheroids. The confocal microscope was used for the analysis of the 3D spheroids at Days 0 and 7.

Confocal Laser Scanning Microscopy of Spheroids

Following the construction of homo- or heterotypic spheroids using fluorescently labelled cells, the optical sectioning of the spheroids was performed via confocal laser scanning microscope (Leica TCS SP8, Leica Microsystems, Wetzlar, Germany) to observe the spatial organization of the cells within the spheroids together with the distribution of the cells within the heterotypic spheroids. The images were acquired with a dry 10X objective lens. Imaging was performed by taking a series of 8–12 optical sections per spheroid starting from the lower bottom of the spheroid. The size of the Z-section was 20 μm, and the whole Z-sections covered approximately 200 μm of the spheroids. All individual images of the Z-sections were used to generate 2D maximum projection images of the spheroids. In our study, white light laser (WLL) was used as the light source and a suitable filter for the RFP-red cells was selected with emission wavelengths of 580–640 nm and for the DIO-green cells with the emission wavelengths of 500–530 nm. The image size was 1024 × 1024 pixels (1.272 × 1.272 μm).

RNA Extraction from the Spheroids

Total RNA was extracted on Days 0, 3 and 7 from the different forms of the spheroids by the Trizol reagent (15596018, Life Technologies GmbH, Darmstadt, Germany) according to the manufacturer's instructions. In brief, the spheroids were collected in a 1.5 mL Eppendorf tube, gently washed with 1X PBS, dissolved in 200 μL of 1X Trypsin for 15 min at 4 °C and centrifuged at 500 × g for 5 min at 4 °C for further RNA isolation. The quality of the RNA was measured using NanoDrop One spectrophotometer (13-400-518, Thermo Fisher Scientific, Darmstadt, Germany). Next, complementary DNA (cDNA) was prepared from 500 ng of total RNA using the Biozym cDNA synthesis kit (331470l, Biozym Scientific GmbH, Hessisch Oldendorf, Germany) following the manufacturer's instructions.

Quantitative Real-Time Polymerase Chain Reaction (RT-qPCR) of Pro-Metastatic Genes

RT-qPCR was carried out in LightCycler 96 Real-Time PCR System (05815916001, Roche Diagnostics AG, Rotkreuz, Switzerland) using GoTaq® Probe qPCR system (A6102, Promega GmBH, Walldorf, Germany) according to the manufacturer's instructions. The relative quantification of target genes was calculated in relation to the hypoxanthine phosphoribosyltransferase 1 (*HPRT-1*) as the reference gene. The relative expression ratio was calculated by the Roche Light cycler software, in which the PCR efficiency value was set to 2. All samples were run in three independent biological replicates. Primers used in our experiments were Prime Time Std qPCR Assay purchased from Integrated DNA Technologies (IDT, Leuven, Belgium; HPRT-1 Hs.PT.58v.45621572, RANKL Hs.PT.58.23324760, IL-6 Hs.PT.58.40226675, MMP-13 Hs.PT.58.40735012, PTHrp Hs.PT.58.41054442).

The primer sequences were as follows: hypoxanthine phosphoribosyltransferase 1 (*HPRT-1*), forward: 5′-TTGTTGTAGGATATGCCCTTGA-3′ and reverse: 5′-GCGATGTCAATAGGACTCCAG-3′; receptor activator of nuclear factor kappa-B ligand (*RANKL*), forward: 5′-AGGAGCTGTGCAAAAGGAAT-3′ and reverse: 5′-TGAGATGAGCAAAAGGCTGAG-3′; interleukin 6 (*IL-6*), forward: 5′GCAGATGAGTACAAAAGTCCTGA-3′ and reverse: 5′-TTCTGTGCCTGCAGCTTC-3′; matrix metalloproteinase 13 (*MMP-13*), forward: 5′-AGCCACTTTATGCTTCCTGA-3′ and reverse: 5′-TGGCATCAAGGGATAAGGAAG-3′; parathyroid hormone-related protein (*PTHrp*), forward: 5′-GTGTTCCTGCTGAGCTACG-3′ and reverse: 5′-GTCATGGAGGAGCTGATGTTC-3′.

Statistical Analysis

Shapiro–Wilk test and Q-Q plots were used to test the distribution and normality of the data. The results were presented as mean ± standard deviation (SD) or mean ± standard error of the mean (SEM). Sample size for growth kinetics, live/dead and confocal microscopy was calculated by G*Power software (version 3.1.9.7, Heinrich-Heine-University, Düsseldorf, Germany) [28] using power analysis to ensure adequate statistical power to the significant results, where primary results of change in size of the spheroids were used to estimate the effect size with significance level set at 0.05 and a desired power of 0.8. The required sample size per group was 6 samples and with calculating 10 % of failure of spheroidization, the sample size was increased to 8 spheroids per group. Statistical analysis was performed by GraphPad Prism software version 9.3.1 (GraphPad Software, San Diego, CA, USA, https://www.graphpad.com/) using two-way repeated measure analysis of variance (ANOVA) followed by Sidak's post-hoc test to determine the significant difference between groups. The significance level was indicated at * $p < 0.05$, ** $p < 0.01$, *** $p < 0.001$ and **** $p < 0.0001$.

Results

The Liquid Overlay Technique on ULA Microplates with Centrifugation was Suitable for the Generation of and Heterotypic MDA-MB-231 Spheroids

To better understand how the tumour interacts with the surrounding environment and to assess the tumour growth model, we have designed an *in vitro* technique based on liquid overlay on ULA microplates with centrifugation as described above. Homotypic bone and breast cancer spheroids and heterotypic tumour spheroids were evaluated in terms of morphology and viability to mimic the physiological conditions.

We established a three-dimensional (3D) spheroid model that can physiologically imitate metastatic bone tumour architecture. To this end, three different multicellular spheroid models were constructed, each containing either the MDA-MB-231 cancer cell line (MDA), human osteoblasts (hOBs), or both cell types with the addition of Matrigel as follows: (i) Control group, in which the spheroids were generated without Matrigel added to the culture medium; (ii) 1 % Matrigel within the spheroid culture medium and (iii) 3.5 % Matrigel added to the culture medium.

A seeding density of 1×10^4 cells/spheroid was selected as the optimum cell density for spheroid formation, based on previous viability assay experiments (results not shown). For the heterotypic spheroids, the ratio of cancer cells to osteoblasts was optimized to 1:1. After the cells were seeded into the ULA microplates and centrifuged, spheroids were formed within 3 days, as observed via phase contrast microscopy. The third day of cell culture was considered the initial day of spheroid formation (Day 0).

Increasing Matrigel Concentration Enhances Spheroid Circularity

The growth of the spheroids related to each condition was monitored by phase-contrast imaging over 14 days and analysed quantitatively (Fig. 1). The ideal spheroid was recognized as a uniform round-shaped translucent ball of cell aggregates with a dark core and defined outer boundaries, which increased in dimension.

Among the homotypic MDA spheroids, those in the control group failed to grow steadily in size over 14 days (Fig. 1**a**). Instead, the size of spheroids decreased from Day 0 (778 ± 71 μm) to Day 7 (639 ± 39 μm). Afterwards, an increase in size was observed on Day 14 (777 ± 58 μm) (Fig. 1**b**). In the Matrigel groups (1 % and 3.5 % Matrigel), uniform spheroids were observed from Day 0 (Fig. 1**a**), but the spheroids in the group containing 3.5 % Matrigel were smaller compared with the 1 % group (647 ± 21 μm vs 723 ± 53 μm) and started to gradually increase in size until Day 14, with diameters of 1094 ± 30 μm and 1112 ± 30 μm, respectively (Fig. 1**b**).

Among the homotypic osteoblasts, it was clear that the spheroids in the control group did not increase in size over time (465 ± 60 μm at Day 0, 398 ± 34 μm at Day 14) (Fig. 1**d,e**). However, in the other groups (1 % and 3.5 % Matrigel), the diameter of the spheroids increased significantly over time from 498 ± 25 μm and 617 ± 50 μm at Day 0 respectively to 926 ± 95 μm and 1425 ± 71 μm at Day 14 respectively (Fig. 1**e**). The rate of diameter increase was related to the concentration of Matrigel.

Among the heterotypic spheroids, the size of the spheroids in the control group decreased over time from 496 ± 50 μm at Day 0 to 369 ± 30 μm at Day 14 (Fig. 1**g,h**). On the contrary, the diameter of spheroids enriched with 1 and 3.5 % Matrigel increased gradually from 615 ± 95 μm and 633 ± 30 μm on Day 0 respectively to 1009 ± 50 μm and 1087 ± 30 μm at Day 14 respectively (Fig. 1**h**).

The optimized seeding density for all three types of spheroids was 1×10^4 /microwell. However, the homo-

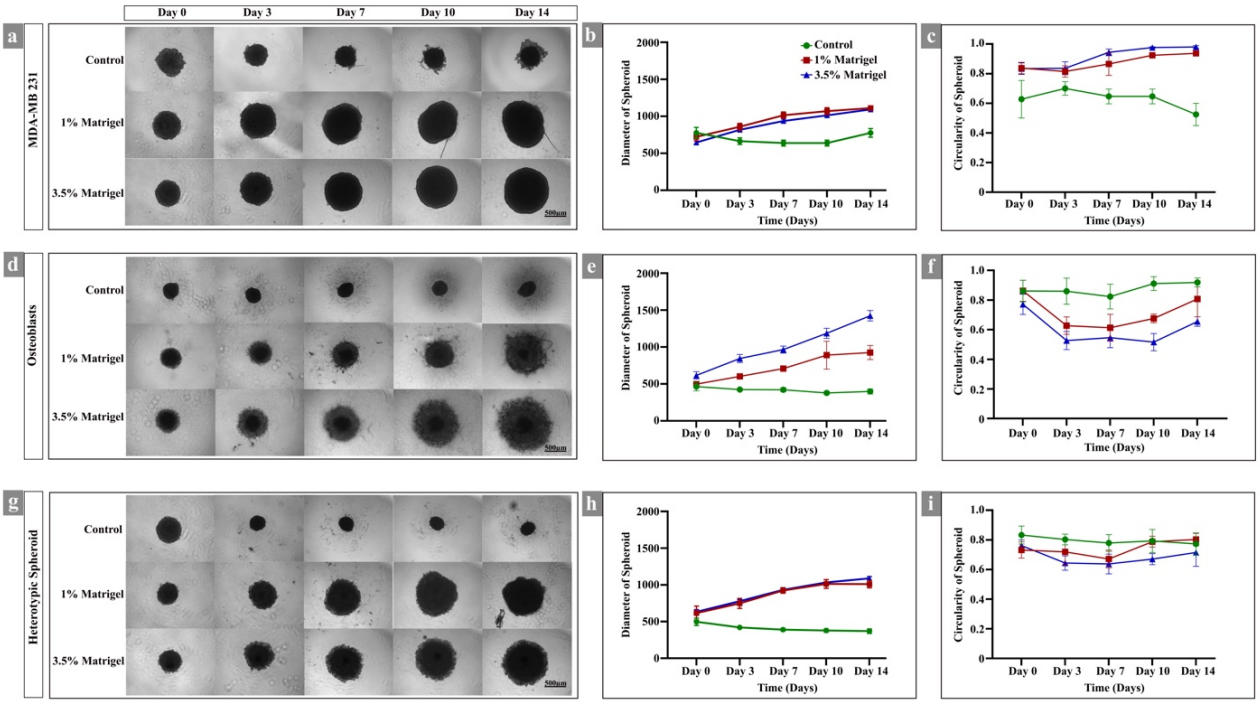

Fig. 1. Morphology and growth kinetics of human spheroids represented as spheroid diameter (μm) at an optimized seeding density of 10,000/spheroid over 14 days using 1 % and 3.5 % Matrigel. Spheroids without Matrigel served as control. Shape parameters represented as circularity index and quantified using ImageJ software. (**a**) Representative images of Homotypic MDA-MB-231 spheroids. (**b**) Growth kinetics of Homotypic MDA-MB-231 spheroids. (**c**) Circularity index of Homotypic MDA-MB-231 spheroids. (**d**) Representative images of Homotypic Primary human Osteoblasts. (**e**) Growth kinetics of Homotypic Primary human Osteoblasts spheroids. (**f**) Circularity index of Homotypic Primary human Osteoblasts. (**g**) Representative images of Heterotypic spheroids. (**h**) Growth kinetics of Heterotypic spheroids. (**i**) Circularity index of Heterotypic spheroids. Data is shown as mean ± SD (n = 8 per group). Scale bar = 500 μm for all the relevant sub-figures. MDA-MB-231, breast adenocarcinoma cell line; SD, standard deviation. Images were taken with 5X objective lens. The figures were generated using Adobe Photoshop (Version 24.1.1, Adobe Inc. (2023). Retrieved from https://www.adobe.com/products/photoshop.html).

typic MDA spheroids formed spheroids with larger diameters than did the hOBs and the heterotypic spheroids. This might be due to the inability of MDA to form tight cellular junctions.

Our results revealed that the circularity index of the spheroids was different among the three groups. In the homotypic MDA spheroids, Matrigel clearly enhanced the circularity of the spheroids, whereas in the control group, the cells were loose aggregates without actual spheroids formation. On Day 14, the groups with 1 % and 3.5 % Matrigel had high circularity indices of 0.93 ± 0.01 and 0.98 ± 0.01 respectively in the formed spheroids compared with those of the control group (0.53 ± 0.07) (Fig. 1**a,c**). In the homotypic hOBs spheroids, on Day 0, the circularity index was 0.77 ± 0.07 with 3.5 % Matrigel whereas it was 0.86 ± 0.07 in both the control group and 1 % Matrigel group. However, the Matrigel groups started showing lower circularity from Day 3. This decline was pronounced in the 3.5 % Matrigel group (Cir = 0.655 ± 0.032) (Fig. 1**d,f**).

In the heterotypic spheroids, the circularity indices of both groups with added Matrigel were comparable. This observation suggested that adding Matrigel to the co-culture of both cell types had a weaker effect on the morphology of the formed spheroids (Fig. 1**g,i**). Inter-group comparisons at the different timepoints for MDA-MB-231 cells, osteoblasts and heterotypic spheroids were provided in **Supplementary Material**.

Matrigel Affects the Viability of the cells According to Live/Dead Imaging of the Spheroids

To analyse the effects of varying concentrations of Matrigel on the viability of the spheroid, a live/dead assay was performed at Days 0 and 7 of spheroid formation (Fig. 2). Viable cells stained green, while non-viable cells took up the red stain, indicating compromised cell membrane integrity.

The viability of the MDA cells was compromised as the spheroids were more compact with 3.5 % Matrigel. However, the cells remained viable at the periphery of the spheroid (Fig. 2**a**).

On the contrary, the viability of the hOBs spheroids was compromised in the control group in which the ra-

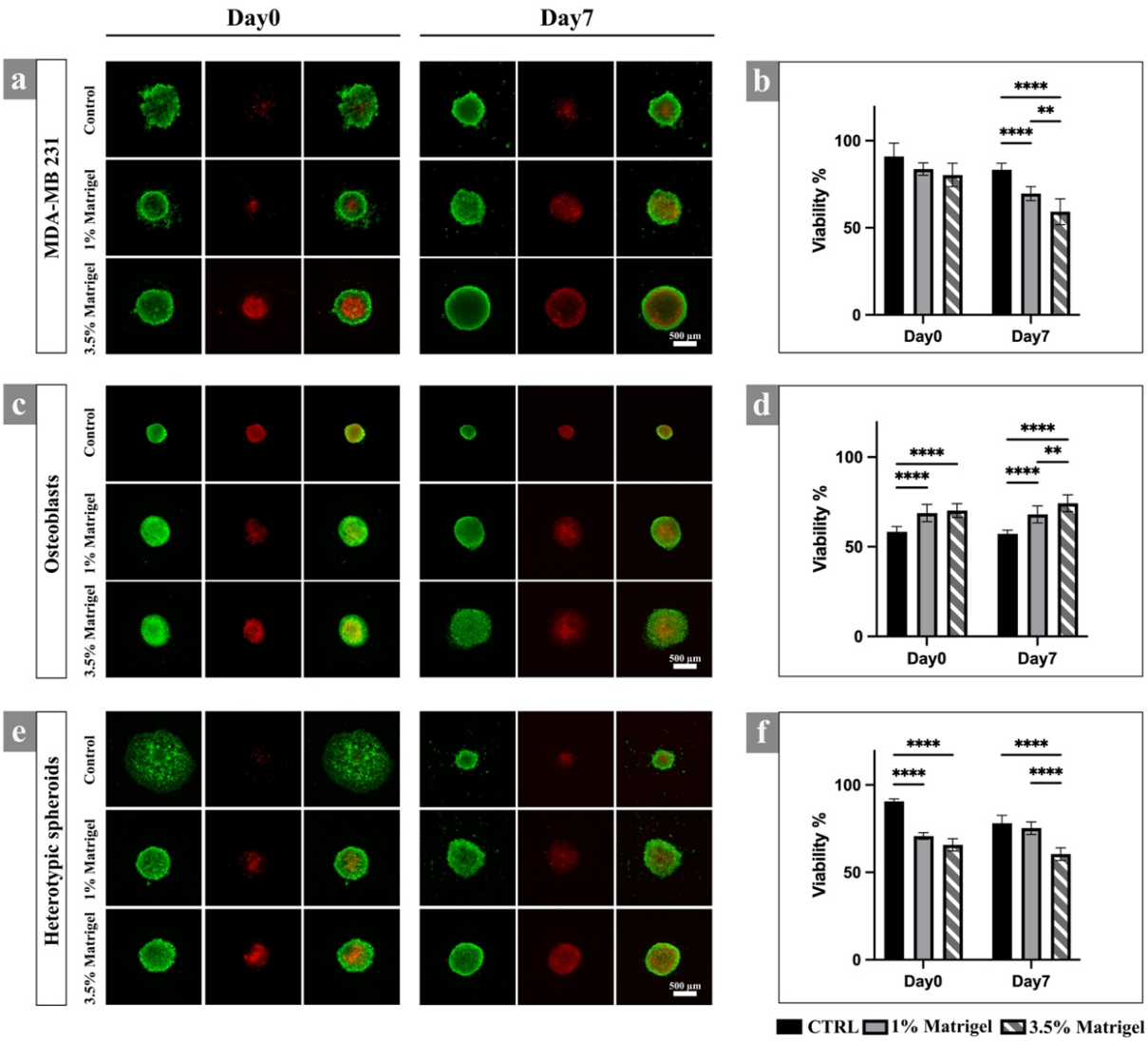

Fig. 2. Cell viability was detected by live/dead staining of the spheroids on Days 0 and 7. (**a**) Fluorescent microscope images of Homotypic MDA-MB-231 spheroids stained with Calcein-AM (Green, viable cells) and Ethidium homodimer-1 (Red, dead cells). (**b**) Quantification of Homotypic MDA-MB-231 spheroids viability expressed as a percentage of viable cells. (**c**) Fluorescent microscope images of Homotypic Primary human Osteoblasts stained with Calcein-AM (Green, viable cells) and Ethidium homodimer-1 (Red, dead cells). (**d**) Quantification of Homotypic Primary human Osteoblasts spheroids viability expressed as a percentage of viable cells. (**e**) Fluorescent microscope images of Heterotypic spheroids stained with Calcein-AM (Green, viable cells) and Ethidium homodimer-1 (Red, dead cells). (**f**) Quantification of Heterotypic spheroids viability expressed as a percentage of viable cells. Data is shown as mean ± SD (n = 8 per group). Images were taken with 10X objective lens. Scale bar = 500 μm for all the relevant sub-figures. The statistical significance was calculated at $^{**}p < 0.01$ and $^{****}p < 0.0001$. Calcein-AM, Calcein acetoxymethylester. The figures were generated using Adobe Photoshop (Version 24.1.1, Adobe Inc. (2023). Retrieved from https://www.adobe.com/products/photoshop.html).

tio of dead cells to the living cells was approximately 1:1, whereas with the addition of Matrigel, the percentage of living cells was greater (Fig. 2**c**).

The heterotypic spheroids formed with 3.5 % Matrigel followed the same pattern as the MDA spheroids. Nevertheless, there was no significant difference in the percentage of viable cells between the control group and the 1.5 % Matrigel on Day 7 (Fig. 2**e**).

The Quantitative Analysis of the Spheroid's Viability Revealed the Following Findings

Among the homotypic MDA spheroids, the viability of the spheroids in the control group remained above 80 % until Day 7. This percentage decreased with the addition of Matrigel to the spheroid culture, in which the viability of spheroids was 68 % at 1 % Matrigel and 60 % at 3.5 % Matrigel on Day 7. Viable cells remained at the periphery, while a dead core was observed at the centre of

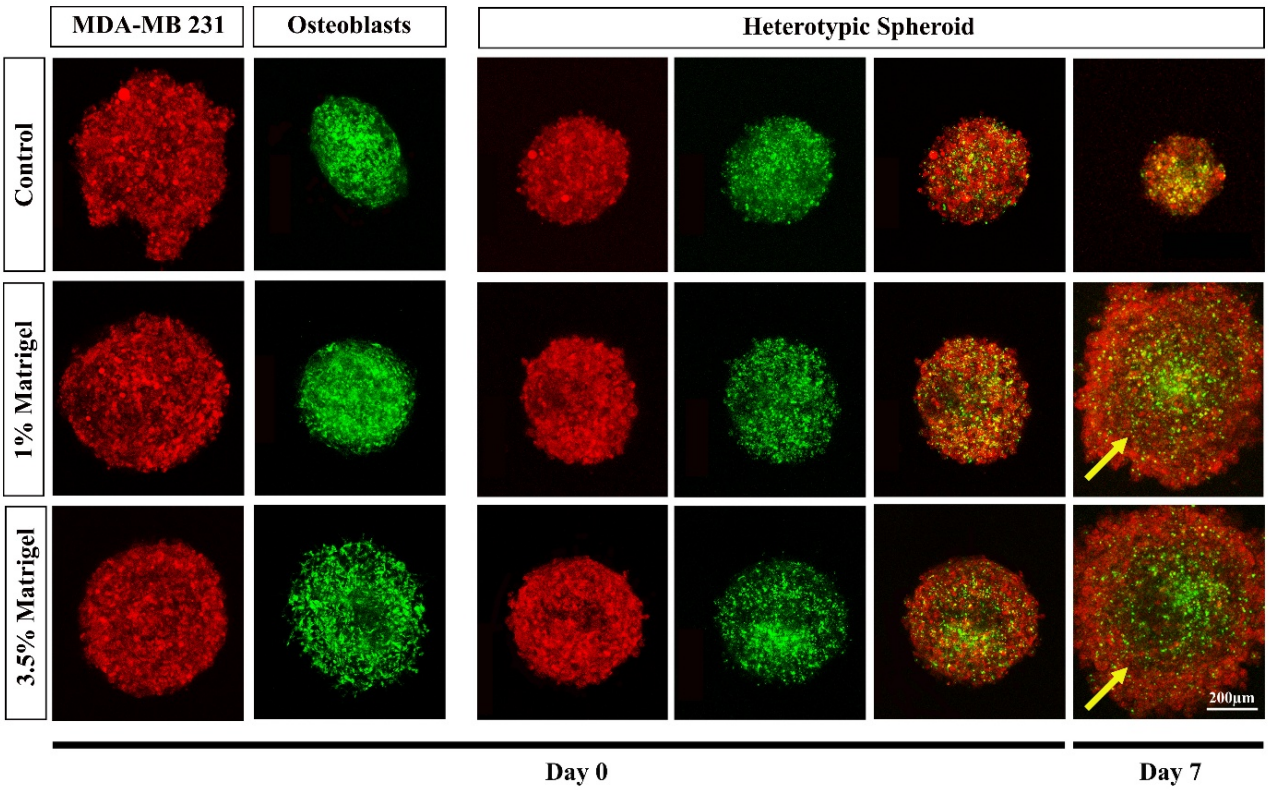

Fig. 3. Confocal Laser scanning Micrographs showing the spatial organization of the cells within spheroids. Red cells represent RFP-expressing MDA-MB-231cells, and green cells represent DIO-labelled hOBs captured with red and green channels. Cellular distribution within the heterotypic spheroids is shown at Days 0 and 7 using images with both red and green channels. Maximum projection images were generated from 8–11 Z-sections for each spheroid using the LAS-X software. Z section = 20 μm. Scale bar = 200 μm for all the relevant sub-figures. Yellow arrows showed the outwards migration of cancer cells away from the center of the spheroid resulting in cellular reorganization within the heterotypic spheroids. hOBs, human osteoblasts; RFP, red fluorescent protein; DIO, 3,3′-Dioctadecyloxacarbocyanine perchlorate. The figures were generated using Adobe Photoshop (Version 24.1.1, Adobe Inc. (2023). Retrieved from https://www.adobe.com/products/photoshop.html).

the spheroids. These results might be due to the increased density of spheroids with increasing Matrigel concentration (Fig. 2**b**).

Among the homotypic hOBs spheroids, the viability of the spheroids in the control group was markedly reduced to 58 % starting as early as Day 0 of spheroid formation. Compared with the control, adding Matrigel to hOBs spheroids significantly improved the viability ($p < 0.0001$). On Day 7, significant differences in the viability of the spheroids were also observed between the low (1 %) and high Matrigel concentration (3.5 %) ($p = 0.01$) (Fig. 2**d**).

For the heterotypic spheroids, the viability of the spheroids followed the same trend as homotypic MDA spheroids, in which increasing the Matrigel concentration negatively affected the viability of the formed spheroids. On Day 7, a significant reduction in viability was observed in the 3.5 % Matrigel group compared with the control group ($p < 0.0001$) (Fig. 2**f**).

Spatial Organisation of the Cells within the Homotypic and Heterotypic Spheroids via Confocal Laser Scanning Microscope

Optical sectioning of the formed spheroids using the confocal microscope performed on Days 0 and 7 of spheroid formation with red RFP-expressing MDA cells and green DIO-labelled hOBs spheroids allowing the study of the effect of Matrigel on the compactness and the spatial organization of the cells within the homotypic and heterotypic spheroids (Fig. 3).

Compared with the control MDA spheroids, the MDA spheroids with Matrigel exhibited tighter aggregation and a more uniform structure. In contrast, the effect of the Matrigel on hOBs spheroids was quite the opposite as hOBs spheroids with Matrigel were less compact than the control spheroids. Compared with the control hOBs spheroids, hOBs on the periphery of the spheroids appeared more elongated, and the spaces between the cells were more expansive.

The co-culture of MDA and hOBs in the heterotypic spheroids resulted in uniformly structured spheroids. Ini-

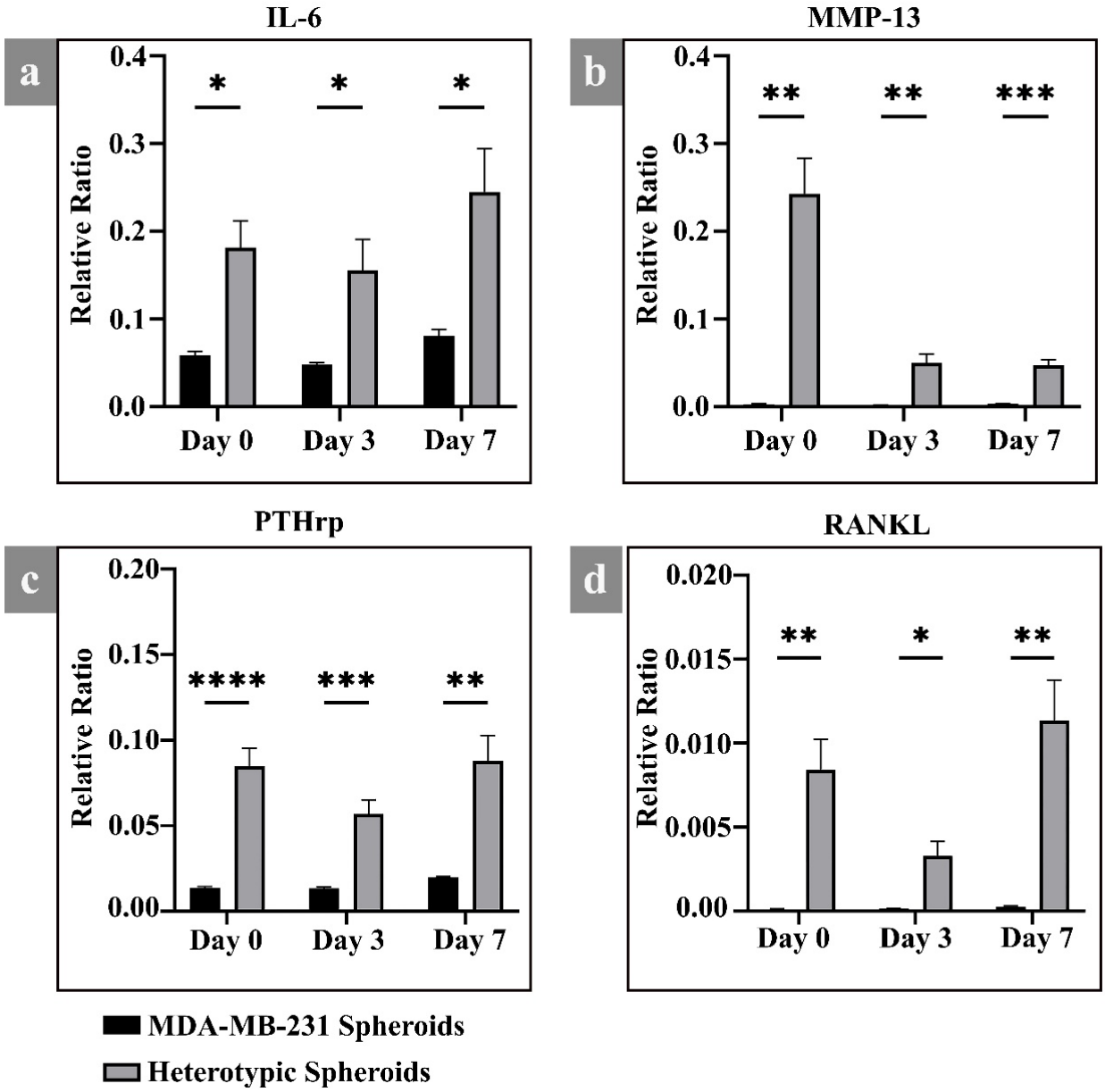

Fig. 4. Relative expression of pro-metastatic genes in heterotypic spheroids versus MDA spheroids on Days 0, 3, 7. RT-qPCR was performed to determine the relative ratio of (**a**) interleukin 6 (*IL-6*). (**b**) Matrix metalloproteinase 13 (*MMP-13*). (**c**) Parathyroid hormone-related protein (*PTHrp*). (**d**) Receptor activator of nuclear factor kappa-B ligand (*RANKL*). *HPRT-1* served as the reference gene. Data were presented as mean ± SEM. The level of significance was indicated at * $p < 0.05$, ** $p < 0.01$, *** $p < 0.001$, **** $p < 0.0001$. RT-qPCR, quantitative real-time polymerase chain reaction; *HPRT-1*, hypoxanthine phosphoribosyltransferase 1; SEM, standard error of the mean. The figures were generated using Adobe Photoshop (Version 24.1.1, Adobe Inc. (2023). Retrieved from https://www.adobe.com/products/photoshop.html).

tially, the cells were organised in a mixed pattern on Day 0. By Day 7, cellular re-organization was observed such that MDA cells had migrated to the periphery and that the osteoblast had migrated to the centre. This phenomenon was particularly pronounced in the Matrigel groups. Moreover, there was a noticeable increase in the spheroid size compared to that of the control group, which was further confirmed via the growth kinetics analysis.

Characterization of the Pro-Metastatic Properties of Heterotypic Spheroids via RNA Extraction and RT-qPCR

To characterize the pro-metastatic properties of the heterotypic spheroids, the spheroid model with 1 % Matrigel was chosen as the optimum model, which represented our bone metastasis model for use in our further drug testing experiments due to the improved viability and circularity of the spheroids. The relative expression of pro-

metastatic genes (*IL-6*, *RANKL*, *MMP-13* and *PTHrp*) in the heterotypic spheroids was compared to that in the homotypic MDA spheroids (Fig. 4).

Compared with that in the homotypic MDA spheroids, the expression of the pro-inflammatory gene (*IL-6*) was upregulated from Day 0 of heterotypic spheroid formation until Day 7 ($p = 0.02$). Moreover, the pro-metastatic genes (*RANKL* and *PTHrp*) were significantly upregulated in the heterotypic spheroids. Significant overexpression of *PTHrp* was detected on Day 0 ($p < 0.0001$) and the level of *PTHrp* decreased relatively over time. In addition, the expression of *MMP-13* gene, which encodes an essential proteolytic enzyme and is a substantial indicator of metastasis and bone degradation, was markedly upregulated until Day 7 ($p = 0.0005$).

Discussion

The fight against cancer has been an ongoing battle for decades. The failure rate of therapy for late-stage cancer is strikingly high, especially for metastatic breast cancer. Although treatment outcomes for primary breast cancer have improved, improvements in metastatic breast cancer are not satisfactory. The successful management of metastatic breast cancer depends primarily on the thorough and reliable preclinical models that can simulate the tumour architecture [29,30].

It is becoming increasingly clear that conventional cancer cell lines grown in monolayers cannot accurately simulate *in vivo* tumour conditions. Accordingly, complex 3D *in vitro* models have been introduced to overcome the overestimation of the effectiveness of chemotherapeutic drugs in 2D models, leading to a new standard that simulates not only tumour cells but also the extracellular matrix [31,32].

It has been well established that the 3D microenvironment alters a range of cellular and functional activities, including proliferation, migration, differentiation, viability, hypoxic zones and drug sensitivity, which can be extrapolated to clinical practice [33].

Multicellular tumour spheroids (MCTSs), an example of the 3D *in vitro* culture, have become a vital tool for preclinical cancer models, as cell aggregation enhances cell-cell and cell-ECM interactions and mimics tumour architecture. They have also been shown to enable a more accurate assessment of the drug efficacy, as spheroids exhibit greater resistance to cancer therapies than conventional 2D cultures by recapitulating many features of the actual cancer microenvironment [34,35]. Therefore, we have chosen this model to be relevant to the clinical outcomes. However, the uniformity in size and shape, the reproducibility of the spheroid culture, and drug penetration into the compact spheroids are challenges that need to be addressed to increase the predictive power of these valuable models [20].

In cancer biology, tumour spheroids are well-established 3D models, but they pose a significant burden to researchers as the methods to generate such spheroids are difficult to standardize [36]. In our study, we have implemented the construction, optimization, and validation of a complex 3D tumour spheroid model to investigate its potential feasibility for future drug screening, which is commonly carried out as an end-point to examine the sensitivity of drugs in cancer cell lines. Our model represents different aspects of metastatic breast cancer by utilising the breast cancer cell line MDA-MB-231 to create homotypic breast cancer spheroids, primary human osteoblasts to generate homotypic bone tissue spheroids, or the 1:1 co-culture of MDA-MB-231 and primary osteoblasts representing breast cancer metastasis to bone (heterotypic tumour spheroids).

To develop each type of spheroid, cells were seeded on ultra-low attachment plates with the addition of a Matrigel matrix to provide structural support for the cells after forced aggregation by centrifugation. We have altered the concentration of the Matrigel while fixing all other factors of culture to study its effect on model characteristics, such as generation time, morphological features, cell viability and gene expression.

In particular, we used MDA-MB-231 cells, a highly destructive triple-negative breast cancer cell line that does not express progesterone or estrogen receptors or human epidermal growth factor receptor 2 (HER2) protein, making these cells insensitive to treatments and resulting in a poorer prognosis than other types of breast cancer [37]. Although the MDA-MB-231 cell line has several advantages, such as relative ease of culture and purity of cancer cells, it is a non-spheroid forming cell line giving only loose aggregates in 3D models due to its natural lack of E-cadherin expression, which limits the ability of cells to spontaneously arrange into compact spheroids [38–40]. Various studies have reported that the addition of supportive scaffold material is needed to augment the compactness of these cancer cells [40,41].

The ECM is a complex 3D network of proteins and polysaccharides that support tissue structure and integrity. The ECM not only passively provides a scaffold for the cells but also regulates cellular functions and plays an essential role in healthy tissue homeostasis and disease progression [42]. Various biomaterials, such as hyaluronic acid, collagen, alginate, chitosan, and Matrigel, have been used as additives for 3D spheroid models to simulate the ECM [43]. Matrigel is a basement membrane extract prepared from engelbreth-holmswarm (EHS) mouse sarcoma and primarily contains laminins, collagen IV, enactin/nidogen, proteoglycans and numerous growth factors [40].

In our experiments, two different techniques have been adopted for tumour spheroid formation with slight modifications [41,44] as MDA cells were able to aggregate upon centrifugation but were incapable of forming compact spheroids on ultra-low attachment plates. However, in the presence of Matrigel (1 % or 3.5 %) the cells enhancing the compactness of the cells, and the cellular functions im-

proved within the 3D spheroids. Moreover, the addition of Matrigel improved the consistency and reproducibility of spheroid formation of MDA cells accompanied by increasing spheroid size over two weeks. It is also worth mentioning that adding 1 % Matrigel was optimal for enhancing the uniformity of MDA spheroids without greatly reducing cell viability.

Human osteoblast spheroids are important for the assessment of metastatic breast cancer in bone, particularly in drug screening studies, as such cell constructs represent normal bone function and remodeling [32]. In our study, primary human osteoblast spheroids were used to simulate the *in vivo* characteristics of the osteoblasts and reflect their typical signaling pathways. The presence of osteoblasts promotes structural changes, migratory behavior and drug resistance of breast cancer cells in a physiologically relevant 3D matrix [45]. The findings suggest that a 3D heterotypic cancer spheroid is a promising model for studying breast cancer bone metastasis because it facilitates the investigation of direct interactions between breast cancer cells and bone cells [46]. Unlike MDA cells, primary human osteoblasts can aggregate rapidly into spheroids. Although the aggregation of osteoblasts into densely compacted spheroids is associated with reduced viability, we demonstrated that the addition of Matrigel significantly improved spheroid viability.

It has been previously reported that aggregation of the osteoblast precursor cells in a scaffold-free, non-osteoinductive culture system induced cell cycle arrest, resulting in inhibition of proliferation and triggering spontaneous differentiation to osteocytes [47]. It has also been reported that the development of spheroids from human-induced pluripotent stem cells with relatively large sizes (>450 μm) is challenging due to the high degree of compaction and impeded oxygen and nutrient diffusion into the spheroid interior [48].

In our homotypic hOB spheroids, the addition of Matrigel provided a substrate for the attachment of osteoblasts and increased their viability over a long period of spheroid culture, mimicking *in vivo* conditions, and affected the phenotypic characteristics of the osteoblasts, especially at the periphery of the spheroids, where the cells were more elongated and spaced apart. Over time, we observed further expansion of the osteoblasts at the periphery of the spheroids, which was significantly more pronounced with a higher concentration of Matrigel. This may be due to increased proliferation and integrin-mediated migration of osteoblasts at the periphery.

The co-culture of breast cancer cells and osteoblasts to form 3D spheroids that represent an *in vitro* bone metastasis model was the final aim of this study. We assessed morphological characteristics and cellular functions, such as viability within the heterotypic spheroids. The MDA-MB-231: hOB ratio was optimized to 1:1 based on previous experiments on cell viability. Although the cellular suspensions were prepared by mixing both cell populations, structural reorganisations of the cells were observed later in culture, suggesting a mutual interaction between osteoblasts and cancer cells. This interaction is thought to enhance tumour growth [49], and our work emphasizes the important mediating role of the ECM in cancer cell-osteoblast interactions. We also observed that the size of the heterotypic spheroids increased significantly with the addition of Matrigel and that a lower concentration of Matrigel (1 %) promoted better viability of the spheroids with smaller necrotic core areas.

This model can be a surrogate for osteolytic bone metastasis by reflecting the elevated gene expression levels of *IL-6*, *PTHrp*, *RANKL* and the matrix degradation marker *MMP-13*. Interleukin-6 has been previously reported to be elevated in the serum of patients with breast cancer bone metastasis and had been associated with poor prognosis and increased cancer aggressiveness [50]. Elevated expression of *IL-6* has been related to interaction between osteoblasts and breast cancer cells [51]. Parathyroid hormone-related protein is a marker for the osteolytic type of bone metastasis and is upregulated when metastatic breast cancer cells become activated in the bone. The production of *PTHrp*, in turn stimulates the production of *RANKL*, the main mediator for osteoclast maturation and activation [52]. Our results showed that the heterotypic model mimics these mechanisms increasing *IL-6*, *PTHrp* and *RANKL* gene expression compared to that in homotypic MDA-MB-231 spheroids. *MMP-13*, which is produced in human breast cancer bone metastasis and is associated with poor patient prognosis [53], was also upregulated at the RNA level in our heterotypic spheroid model.

The advantages of our spheroid model lie in its ability to simulate the bone microenvironment through the interaction between breast cancer cells and osteoblasts. In addition, the incorporation of Matrigel as an ECM material further stimulates these interactions, which markedly increases the biological relevance of our model compared to 3D spheroid systems lacking heterotypic cellular populations or added ECM materials. With the application of this model, more precise predictions of drug responses are expected. Additionally, the improved feasibility and uniformity of the size and shape of the spheroids produced under our protocol facilitate their use in high-throughput drug screening applications, which in turn further strengthens the model's applicability. Furthermore, the versatility of the proposed workflow allows for the incorporation of diverse cellular populations and various ECM materials. This approach effectively reflects both the efficacy of cancer therapies and potential resistance mechanisms.

Although the proposed model has demonstrated promising results, there are some inherent limitations that should be considered when evaluating the findings. Although spheroids present a more physiological platform for drug testing, the MDA-MB-231 cell line did not have the

ability to form spontaneous tumour spheroids. Thus, an additional matrix must be used to form tumour spheroid which was Matrigel in our case. The interaction between the cells and Matrigel resulted in the formation of highly dense spheroids, which reduced the viability of the spheroids and affected the penetration of certain reagents used in the testing assays. This issue was solved by using a lower concentration of Matrigel (1 %), although higher concentrations produced well-formed circular spheroids with a circularity index close to 1. Despite its effectiveness, Matrigel is derived from animal tumour which results in batch-to-batch variability in protein composition. This variability might impact the reproducibility of the model, especially in high-throughput applications where multiple lots may be used. As an alternative to Matrigel, synthetic polymers such as MethoCel, has been explored for their ability to enhance spheroid formation [54], yet natural ECM materials enhance the physiological relevance of the model.

A potential area for future research would be validating the impact of Matrigel on both homotypic and heterotypic spheroid models in drug testing experiments and optimizing the workflows. By applying those workflows in a high throughput setup, the reliability and scalability of the model for drug development and other functional applications can be greatly enhanced. Another area for future research would be the *in vivo* validation of the model by comparing the drug response *in vivo* to that of the spheroid model. This comparison is a crucial step in the assessment of the translational relevance and predictive accuracy of the model.

Conclusions

Bone is a preferable niche for metastatic cancer cells where they disrupt bone homeostasis. 2D monolayer cultures have recently been replaced by 3D tumour models, which allow a better understanding of bone metastasis and provide more accurate results under conditions closer to clinical reality.

In this study, we have constructed 3D heterotypic tumour spheroids using 1 % Matrigel as a robust and versatile model to study different aspects of breast cancer metastasizing to bone for further drug testing. By adjusting the concentration of Matrigel within the spheroid culture, we optimised the culture conditions to achieve minimal impact on viability while ensuring uniformity in the size and morphology of the generated spheroids. Future directions: in our future studies, we plan to test the reliability of the model by performing drug response assays to determine the effect of the drugs on this model. Our tumour spheroid model not only provides a reliable platform for future *in vitro* cell-based drug screening to investigate the cytotoxicity of cancer cells, tolerability of bone cells and the effect of heterogeneous bone-cancer environment on treatment resistance but is also physiologically appropriate for *in vivo* conditions.

List of Abbreviations

3D, three-dimensional; MCTSs, multicellular tumour spheroids; 2D, two-dimensional; ULA, ultra-low attachment; RT-qPCR, quantitative real-time polymerase chain reaction; ECM, extracellular matrix; BC, breast cancer; SREs, skeletal-related events; FDA, Food and Drug Administration; hOBs, human osteoblasts; MDA-MB-231, breast adenocarcinoma cell line; DMEM-HG, Dulbecco's modified Eagle medium high glucose; Cir, circularity; TCCF, total corrected cellular fluorescence; ID, integrated density; FACS, fluorescence-activated cell sorting; WLL, white light laser; *HPRT-1*, hypoxanthine phosphoribosyltransferase 1; *RANKL*, receptor activator of nuclear factor kappa-B ligand; *MMP-13*, matrix metalloproteinase 13; *PTHrp*, parathyroid hormone-related protein; SD, standard deviation; SEM, standard error of the mean; HER2, human epidermal growth factor receptor 2; EHS, engelbreth-holmswarm; IL-6, interleukin 6; Calcein-AM, Calcein acetoxymethylester; PBS, phosphate buffer saline; RFP, red fluorescent protein; DIO, 3,3′-Dioctadecyloxacarbocyanine perchlorate; cDNA, complementary DNA.

Availability of Data and Materials

All data reported in this paper will be shared by the lead contact upon request.

Author Contributions

AA and RF contributed to the design of this work. HN and RF contributed to the analysis and interpretation of data. SO contributed to the interpretation of data. HN drafted the work. AA, SO and RF revised the work critically for important intellectual content. All authors read and approved the final manuscript. All authors agree to be accountable for all aspects of the work in ensuring that questions related to the accuracy or integrity of any part of the work are appropriately investigated and resolved.

Ethics Approval and Consent to Participate

Not applicable.

Acknowledgments

We gratefully acknowledge the assistance of Professor Hanna Taipaleenmäki from the Institute of Musculoskeletal Medicine (IMM) for donating the MDA-MB-231 adenocarcinoma cell line. Furthermore, we would like to thank Dr. Maximilian Saller for his support in the Confocal Laser scanning Microscopy. Additionally, we extend our gratitude to Martina Burggraf for the nucleofection experiments of the RFP-expressing MDA-MB231 cell line.

Funding

This research was funded by Bayerische Forschungsstiftung, grant number AZ DOK-191-21.

Conflict of Interest

The authors declare no conflict of interest.

Supplementary Material

Supplementary material associated with this article can be found, in the online version, at https://doi.org/10.22203/eCM.v052a04.

References

[1] Shao H, Varamini P. Breast Cancer Bone Metastasis: A Narrative Review of Emerging Targeted Drug Delivery Systems. Cells. 2022; 11: 388. https://doi.org/10.3390/cells11030388.

[2] Cosphiadi I, Atmakusumah TD, Siregar NC, Muthalib A, Harahap A, Mansyur M. Bone Metastasis in Advanced Breast Cancer: Analysis of Gene Expression Microarray. Clinical Breast Cancer. 2018; 18: e1117–e1122. https://doi.org/10.1016/j.clbc.2018.03.001.

[3] Akhtar M, Haider A, Rashid S, Al-Nabet ADMH. Paget's "Seed and Soil" Theory of Cancer Metastasis: An Idea Whose Time has Come. Advances in Anatomic Pathology. 2019; 26: 69–74. https://doi.org/10.1097/pap.0000000000000219.

[4] Tesfamariam Y, Jakob T, Wöckel A, Adams A, Weigl A, Monsef I, *et al*. Adjuvant bisphosphonates or RANK-ligand inhibitors for patients with breast cancer and bone metastases: A systematic review and network meta-analysis. Critical Reviews in Oncology/Hematology. 2019; 137: 1–8. https://doi.org/10.1016/j.critrevonc.2019.02.004.

[5] Allemani C, Matsuda T, Di Carlo V, Harewood R, Matz M, Nikšić M, *et al*. Global surveillance of trends in cancer survival 2000-14 (CONCORD-3): analysis of individual records for 37 513 025 patients diagnosed with one of 18 cancers from 322 population-based registries in 71 countries. Lancet. 2018; 391: 1023–1075. https://doi.org/10.1016/s0140-6736(17)33326-3.

[6] Pisani P, Airoldi M, Allais A, Aluffi Valletti P, Battista M, Benazzo M, *et al*. Metastatic disease in head & neck oncology. Acta Otorhinolaryngologica Italica: Organo Ufficiale Della Società Italiana di Otorinolaringologia e Chirurgia Cervico-Facciale. 2020; 40: S1–S86. https://doi.org/10.14639/0392-100X-suppl.1-40-2020.

[7] Gote V, Nookala AR, Bolla PK, Pal D. Drug Resistance in Metastatic Breast Cancer: Tumor Targeted Nanomedicine to the Rescue. International Journal of Molecular Sciences. 2021; 22: 4673. https://doi.org/10.3390/ijms22094673.

[8] Baghban R, Roshangar L, Jahanban-Esfahlan R, Seidi K, Ebrahimi-Kalan A, Jaymand M, *et al*. Tumor microenvironment complexity and therapeutic implications at a glance. Cell Communication and Signaling: CCS. 2020; 18: 59. https://doi.org/10.1186/s12964-020-0530-4.

[9] Lamouline A, Bersini S, Moretti M. *In vitro* models of breast cancer bone metastasis: analyzing drug resistance through the lens of the microenvironment. Frontiers in Oncology. 2023; 13: 1135401. https://doi.org/10.3389/fonc.2023.1135401.

[10] Carvalho V, Bañobre-López M, Minas G, Teixeira SFCF, Lima R, Rodrigues RO. The integration of spheroids and organoids into organ-on-a-chip platforms for tumour research: A review. Bioprinting. 2022; 27: e00224. https://doi.org/https://doi.org/10.1016/j.bprint.2022.e00224.

[11] Simmons JK, Hildreth BE 3rd, Supsavhad W, Elshafae SM, Hassan BB, Dirksen WP, *et al*. Animal Models of Bone Metastasis. Veterinary Pathology. 2015; 52: 827–841. https://doi.org/10.1177/0300985815586223.

[12] Kolahi Azar H, Gharibshahian M, Rostami M, Mansouri V, Sabouri L, Beheshtizadeh N, *et al.* The progressive trend of modeling and drug screening systems of breast cancer bone metastasis. Journal of Biological Engineering. 2024; 18: 14. https://doi.org/10.1186/s13036-024-00408-5.

[13] Ingber DE. Human organs-on-chips for disease modelling, drug development and personalized medicine. Nature Reviews. Genetics. 2022; 23: 467–491. https://doi.org/10.1038/s41576-022-00466-9.

[14] Subia B, Dahiya UR, Mishra S, Ayache J, Casquillas GV, Caballero D, *et al*. Breast tumor-on-chip models: From disease modeling to personalized drug screening. Journal of Controlled Release: Official Journal of the Controlled Release Society. 2021; 331: 103–120. https://doi.org/10.1016/j.jconrel.2020.12.057.

[15] Pathi SP, Kowalczewski C, Tadipatri R, Fischbach C. A novel 3-D mineralized tumor model to study breast cancer bone metastasis. PLoS One. 2010; 5: e8849. https://doi.org/10.1371/journal.pone.0008849.

[16] Hong S, Song JM. 3D bioprinted drug-resistant breast cancer spheroids for quantitative *in situ* evaluation of drug resistance. Acta Biomaterialia. 2022; 138: 228–239. https://doi.org/10.1016/j.actbio.2021.10.031.

[17] Kaur G, Evans DM, Teicher BA, Coussens NP. Complex Tumor Spheroids, a Tissue-Mimicking Tumor Model, for Drug Discovery and Precision Medicine. SLAS Discovery: Advancing Life Sciences R & D. 2021; 26: 1298–1314. https://doi.org/10.1177/24725552211038362.

[18] Domingues M, Leite Pereira C, Sarmento B, Castro F. Mimicking 3D breast tumor-stromal interactions to screen novel cancer therapeutics. European Journal of Pharmaceutical Sciences: Official Journal of the European Federation for Pharmaceutical Sciences. 2023; 190: 106560. https://doi.org/10.1016/j.ejps.2023.106560.

[19] Lee SI, Choi YY, Kang SG, Kim TH, Choi JW, Kim YJ, *et al*. 3D Multicellular Tumor Spheroids in a Microfluidic Droplet System for Investigation of Drug Resistance. Polymers. 2022; 14: 3752. https://doi.org/10.3390/polym14183752.

[20] Han SJ, Kwon S, Kim KS. Challenges of applying multicellular tumor spheroids in preclinical phase. Cancer Cell International. 2021; 21: 152. https://doi.org/10.1186/s12935-021-01853-8.

[21] Lazzari G, Nicolas V, Matsusaki M, Akashi M, Couvreur P, Mura S. Multicellular spheroid based on a triple co-culture: A novel 3D model to mimic pancreatic tumor complexity. Acta Biomaterialia. 2018; 78: 296–307. https://doi.org/https://doi.org/10.1016/j.actbio.2018.08.008.

[22] Herrmann D, Conway JR, Vennin C, Magenau A, Hughes WE, Morton JP, *et al*. Three-dimensional cancer models mimic cell-matrix interactions in the tumour microenvironment. Carcinogenesis. 2014; 35: 1671–1679. https://doi.org/10.1093/carcin/bgu108.

[23] Qu F, Zhao S, Cheng G, Rahman H, Xiao Q, Chan RWY, *et al*. Double emulsion-pretreated microwell culture for the *in vitro* production of multicellular spheroids and their *in situ* analysis. Microsystems & Nanoengineering. 2021; 7: 38. https://doi.org/10.1038/s41378-021-00267-w.

[24] Capes-Davis A, Theodosopoulos G, Atkin I, Drexler HG, Kohara A, MacLeod RAF, *et al*. Check your cultures! A list of cross-contaminated or misidentified cell lines. International Journal of Cancer. 2010; 127: 1–8. https://doi.org/https://doi.org/10.1002/ijc.25242.

[25] Kelm JM, Timmins NE, Brown CJ, Fussenegger M, Nielsen LK. Method for generation of homogeneous multicellular tumor spheroids applicable to a wide variety of cell types. Biotechnology and Bioengineering. 2003; 83: 173–180. https://doi.org/10.1002/bit.10655.

[26] McCloy RA, Rogers S, Caldon CE, Lorca T, Castro A, Burgess A. Partial inhibition of Cdk1 in G 2 phase overrides the SAC and decouples mitotic events. Cell Cycle. 2014; 13: 1400–1412. https://doi.org/10.4161/cc.28401.

[27] Akova Ölken E, Aszodi A, Taipaleenmäki H, Saito H, Schönitzer V, Chaloupka M, *et al.* SFRP2 Overexpression Induces an Osteoblast-like Phenotype in Prostate Cancer Cells. Cells. 2022; 11: 4081. https://doi.org/10.3390/cells11244081.

[28] Faul F, Erdfelder E, Lang AG, Buchner A. G*Power 3: a flexible

statistical power analysis program for the social, behavioral, and biomedical sciences. Behavior Research Methods. 2007; 39: 175–191. https://doi.org/10.3758/BF03193146.

[29] Boix-Montesinos P, Soriano-Teruel PM, Armiñán A, Orzáez M, Vicent MJ. The past, present, and future of breast cancer models for nanomedicine development. Advanced Drug Delivery Reviews. 2021; 173: 306–330. https://doi.org/10.1016/j.addr.2021.03.018.

[30] Li J, Goh ELK, He J, Li Y, Fan Z, Yu Z, *et al*. Emerging Intrinsic Therapeutic Targets for Metastatic Breast Cancer. Biology. 2023; 12: 697. https://doi.org/10.3390/biology12050697.

[31] Imamura Y, Mukohara T, Shimono Y, Funakoshi Y, Chayahara N, Toyoda M, *et al*. Comparison of 2D- and 3D-culture models as drug-testing platforms in breast cancer. Oncology Reports. 2015; 33: 1837–1843. https://doi.org/10.3892/or.2015.3767.

[32] Marozin S, Simon-Nobbe B, Huth A, Beyerer E, Weber L, Nüssler A, *et al*. Aggregation of human osteoblasts unlocks self-reliant differentiation and constitutes a microenvironment for 3D-co-cultivation with other bone marrow cells. Scientific Reports. 2024; 14: 10345. https://doi.org/10.1038/s41598-024-60986-8.

[33] Huang Z, Yu P, Tang J. Characterization of Triple-Negative Breast Cancer MDA-MB-231 Cell Spheroid Model. OncoTargets and Therapy. 2020; 13: 5395–5405. https://doi.org/10.2147/ott.S249756.

[34] Moradian C, Rahbarizadeh F. PE38-based gene therapy of HER2-positive breast cancer stem cells via VHH-redirected polyamidoamine dendrimers. Scientific Reports. 2021; 11: 15517. https://doi.org/10.1038/s41598-021-93972-5.

[35] Mittler F, Obeïd P, Rulina AV, Haguet V, Gidrol X, Balakirev MY. High-Content Monitoring of Drug Effects in a 3D Spheroid Model. Frontiers in Oncology. 2017; 7: 293. https://doi.org/10.3389/fonc.2017.00293.

[36] Namgung B, Dai H, Prathyushaa Vikraman P, Saha T, Sengupta S, Lin Jang H. An inexpensive "do-it-yourself" device for rapid generation of uniform tumor spheroids. Device. 2024; 2: 100255. https://doi.org/10.1016/j.device.2024.100255.

[37] Saraiva DP, Matias AT, Braga S, Jacinto A, Cabral MG. Establishment of a 3D Co-culture With MDA-MB-231 Breast Cancer Cell Line and Patient-Derived Immune Cells for Application in the Development of Immunotherapies. Frontiers in Oncology. 2020; 10: 1543. https://doi.org/10.3389/fonc.2020.01543.

[38] Manuel Iglesias J, Beloqui I, Garcia-Garcia F, Leis O, Vazquez-Martin A, Eguiara A, *et al*. Mammosphere formation in breast carcinoma cell lines depends upon expression of E-cadherin. PLoS One. 2013; 8: e77281. https://doi.org/10.1371/journal.pone.0077281.

[39] Jokar F, Mahabadi JA, Salimian M, Taherian A, Hayat SMG, Sahebkar A, *et al*. Differential Expression of HSP90β in MDA-MB-231 and MCF-7 Cell Lines after Treatment with Doxorubicin. Journal of Pharmacopuncture. 2019; 22: 28–34. https://doi.org/10.3831/kpi.2019.22.003.

[40] Badea MA, Balas M, Hermenean A, Ciceu A, Herman H, Ionita D, *et al*. Influence of Matrigel on Single- and Multiple-Spheroid Cultures in Breast Cancer Research. SLAS Discovery: Advancing Life Sciences R & D. 2019; 24: 563–578. https://doi.org/https://doi.org/10.1177/2472555219834698.

[41] Froehlich K, Haeger JD, Heger J, Pastuschek J, Photini SM, Yan Y, *et al*. Generation of Multicellular Breast Cancer Tumor Spheroids: Comparison of Different Protocols. Journal of Mammary Gland Biology and Neoplasia. 2016; 21: 89–98. https://doi.org/10.1007/s10911-016-9359-2.

[42] Urciuolo F, Imparato G, Netti PA. *In vitro* strategies for mimicking dynamic cell-ECM reciprocity in 3D culture models. Frontiers in Bioengineering and Biotechnology. 2023; 11: 1197075. https://doi.org/10.3389/fbioe.2023.1197075.

[43] Kamatar A, Gunay G, Acar H. Natural and Synthetic Biomaterials for Engineering Multicellular Tumor Spheroids. Polymers. 2020; 12: 2506. https://doi.org/10.3390/polym12112506.

[44] Nazari SS. Generation of 3D Tumor Spheroids with Encapsulating Basement Membranes for Invasion Studies. Current Protocols in Cell Biology/Editorial Board, Juan S. Bonifacino ... [*et al.*]. 2020; 87: e105. https://doi.org/10.1002/cpcb.105.

[45] Zhu W, Castro NJ, Cui H, Zhou X, Boualam B, McGrane R, *et al*. A 3D printed nano bone matrix for characterization of breast cancer cell and osteoblast interactions. Nanotechnology. 2016; 27: 315103. https://doi.org/10.1088/0957-4484/27/31/315103.

[46] Cui H, Esworthy T, Zhou X, Hann SY, Glazer RI, Li R, *et al.* Engineering a Novel 3D Printed Vascularized Tissue Model for Investigating Breast Cancer Metastasis to Bone. Advanced Healthcare Materials. 2020; 9: e1900924. https://doi.org/10.1002/adhm.201900924.

[47] Kim J, Adachi T. Cell Condensation Triggers the Differentiation of Osteoblast Precursor Cells to Osteocyte-Like Cells. Frontiers in Bioengineering and Biotechnology. 2019; 7: 288. https://doi.org/10.3389/fbioe.2019.00288.

[48] Nath SC, Horie M, Nagamori E, Kino-Oka M. Size- and time-dependent growth properties of human induced pluripotent stem cells in the culture of single aggregate. Journal of Bioscience and Bioengineering. 2017; 124: 469–475. https://doi.org/10.1016/j.jbiosc.2017.05.006.

[49] Zarrer J, Haider MT, Smit DJ, Taipaleenmäki H. Pathological Crosstalk between Metastatic Breast Cancer Cells and the Bone Microenvironment. Biomolecules. 2020; 10: 337. https://doi.org/10.3390/biom10020337.

[50] Lin S, Gan Z, Han K, Yao Y, Min D. Interleukin-6 as a prognostic marker for breast cancer: a meta-analysis. Tumori. 2015; 101: 535–541. https://doi.org/10.5301/tj.5000357.

[51] Haider MT, Ridlmaier N, Smit DJ, Taipaleenmäki H. Interleukins as Mediators of the Tumor Cell—Bone Cell Crosstalk during the Initiation of Breast Cancer Bone Metastasis. International Journal of Molecular Sciences. 2021; 22: 2898. https://doi.org/10.3390/ijms22062898.

[52] Mundy GR. Mechanisms of bone metastasis. Cancer. 1997; 80: 1546–1556. https://doi.org/10.1002/(SICI)1097-0142(19971015)80:8+<1546::AID-CNCR4>3.0.CO;2-I.

[53] Pivetta E, Scapolan M, Pecolo M, Wassermann B, Abu-Rumeileh I, Balestreri L, *et al*. MMP-13 stimulates osteoclast differentiation and activation in tumour breast bone metastases. Breast Cancer Research: BCR. 2011; 13: R105. https://doi.org/10.1186/bcr3047.

[54] Leung BM, Lesher-Perez SC, Matsuoka T, Moraes C, Takayama S. Media additives to promote spheroid circularity and compactness in hanging drop platform. Biomaterials Science. 2015; 3: 336–344. https://doi.org/10.1039/C4BM00319E.

Editor's note: The Scientific Editor responsible for this paper was Chris Evans.

Received: 6th November 2024; **Accepted**: 27th May 2025; **Published**: 23rd July 2025